Physical and Engineering Sciences in Medicine (2022) 45:637–642
https://doi.org/10.1007/s13246-022-01130-6

SCIENTIFIC PAPER

Influence of field of view size and reconstruction methods on single-energy metal artifact reduction: a phantom study

Kunihito Tsuboi[1] · Naoko Osaki[1] · Yuki Ohtani[1] · Ken Tanikawa[1] · Masanori Kaneko[1]

Received: 10 March 2022 / Accepted: 26 April 2022 / Published online: 20 May 2022

Abstract

The purpose of this study was to evaluate the effect of single-energy metal artifact reduction (SEMAR) for metal artifacts using CT images reconstructed with adaptive iterative dose reduction three dimensional (AIDR3D) and advanced intelligent clear-IQ engine (AiCE) in calibration-field of view of various sizes. A prosthetic hip joint was arranged at the center of the phantom. The phantom images were scanned by changing calibration-field of view of 320 mm and 500 mm, and were reconstructed using filtered back-projection (FBP), AIDR3D, and AiCE with and without SEMAR, respectively. The metal artifact reduction with SEMAR was evaluated by calculated the relative artifact index value and visual scores in degree of artifact by seven radiology technologists. Relative artifact index of FBP, AIDR3D, and AiCE with 320 mm/500 mm calibration-field of views were 10.2/10.0, 16.3/16.4, and 17.8/17.9 without SEMAR, 3.3/3.1, 2.6/2.5, and 2.3/2.0 with SEMAR, respectively. Visual scores were not significantly different between 320 and 500 mm calibration-field of views in all reconstruction methods. The effect of metal artifact reduction was not affected by calibration-field of view sizes in the SEMAR combined with AIDR3D or AiCE.

Keywords Computed tomography · SEMAR · Deep learning · Field of view · Artifact

Introduction

Computed tomography (CT) examination is commonly used to detect postoperative total hip arthroplasties (THA). However, metal artifacts from the artificial hip joint in THA patients disturb postoperative diagnosis of surrounding tissues and bones [1]. The cause of metal artifacts are beam-hardening, extensive photon starvation, and scatter [2]. Various methods are used to reduce metal artifacts, including alteration of image reconstruction method [3], scanning with a dual-energy CT [4, 5], and using metal artifact reduction software [1, 3, 5–11].

Single-energy metal artifact reduction (SEMAR; Canon Medical Systems, Otawara, Japan) is a metal artifact reduction software designed for CT scanners of Canon Medical Systems. SEMAR uses a metal inpainting technique that applies forward projections, tissue classification, and back projections in the raw data. It has been reported that SEMAR reduces metal artifacts in various fields such as orthopedics [1, 5–7], endovascular aortic repair devices [11], pacemaker [3], dentistry [6, 8], and coil embolization [6]. On the other hand, it has been reported that SEMAR has a different metal artifact reduction effect depending on the shape of the metal [6], image reconstruction methods [9], and the scan parameters [3, 7, 10]. Andersson et al. [5] have indicated that the creation of new artifacts are particularly obvious when the SEMAR algorithm is combined with iterative reconstruction (IR). Furthermore, it has been shown that the metal artifact reduction effect of SEMAR in CT images reconstructed with filtered back-projection (FBP) is affected by calibration-field of view (C-FOV) size [7]. However, it is not clear whether the metal artifact reduction effect of SEMAR in CT images reconstructed with IR or deep learning reconstruction (DLR) is affected by C-FOV size. In particular, commercially available DLR for CT of Canon, advanced intelligent clear-IQ engine (AiCE, Canon Medical Systems, Otawara, Japan), is trained to differentiate signal from noise and can suppress noise. Therefore, it is necessary to confirm the metal artifact reduction effect using SEMAR combined with AiCE because AiCE may affect artifacts. As a result,

✉ Kunihito Tsuboi
tsuboi-kunihito@gero-hp.jp

[1] Department of Central Radiology, Gifu Prefectural Gero Hot Spring Hospital, 2211 Mori, Gero, Gifu 509-2292, Japan

we investigated the effect of SEMAR on the size of C-FOVs and the choice of reconstruction methods.

The purpose of this study was to evaluate the effect of SEMAR for metal artifacts using CT images reconstructed with DLR and IR in C-FOV of various sizes.

Materials and methods

Phantom design

A cylindrical phantom made from acrylic and artificial hip joint were used in this study (Fig. 1). The diameter and length of the phantom were 216 mm and 186 mm. The artificial hip joint consisted of the alloclassic stem (titanium), the durasul head (alumina ceramic) and the IOI bipolar cup (polyethylene). The artificial hip joint was fixed at the center of the phantom filled with water.

CT image acquisition

The CT images were performed using a 80-detector row CT scanner (Aquilion PRIME SP; Canon Medical Systems, Otawara, Japan) in this study. the CT acquisition parameters were as follows: acquisition mode, helical; gantry rotation time, 0.5 s/rotation; C-FOVs, 320 and 500 mm; tube voltage, 120 kV; tube current, 75 mAs with C-FOV size of 320 mm and 90 mAs with C-FOV size of 500 mm (tube currents of two C-FOV sizes were set to standard deviation (SD) value of 10 for the water CT value of the phantom without artificial hip joint); number of scans, 10. Reconstruction conditions were slice thickness of 5.0 mm, display-FOV of 250 mm, and FC03 kernel (i.e. soft-tissue kernel). CT images were reconstructed with FBP, adaptive iterative dose reduction three dimensional (AIDR3D, Canon Medical Systems, Otawara, Japan), and AiCE, with and without SEMAR, respectively.

Fig. 1 The phantom with artificial hip joint in the center

Objective analysis

Quantitative image analysis was calculated using the free software package ImageJ (NIH) [12]. Rectangle regions of interest (ROIs) were placed around the artificial hip joint and in a metal implant-free slice to measure the standard deviation (SD) of the CT value in these ROIs (Fig. 2). The relative artifact index (AI_r) was calculated using the measured SDs by the following formula:

$$AI_r = \frac{\sqrt{SD_A^2 - SD_B^2}}{SD_B} \quad (1)$$

SD_A and SD_B indicate the SD values around the artificial hip joint and the background SD values, respectively [13].

Takada et al. [13] indicated that AI_r, which divided artifact index (AI) of Eq. (2) by the SD value of the background, can evaluate quantitative artifact amount independent of image noise.

$$AI = \sqrt{SD_A^2 - SD_B^2} \quad (2)$$

AI is defined not by the ratio of SDs in the metal artifact image and the background image, but by the difference between those of SDs [7–10, 13]. Therefore, CT images with high image noise increase the difference between the SDs of the metal artifact image and the SDs of the background image. In other words, it may not be possible to determine whether fluctuations in the AI values are affected by metal artifacts or image noise. In this study, which evaluated metal artifacts by changing the reconstruction methods and C-FOVs size, the image noise of the CT images in this analysis depends on the reconstruction methods and C-FOVs size. Therefore, the AI_r was used to evaluate the degree of metal artifacts in this study.

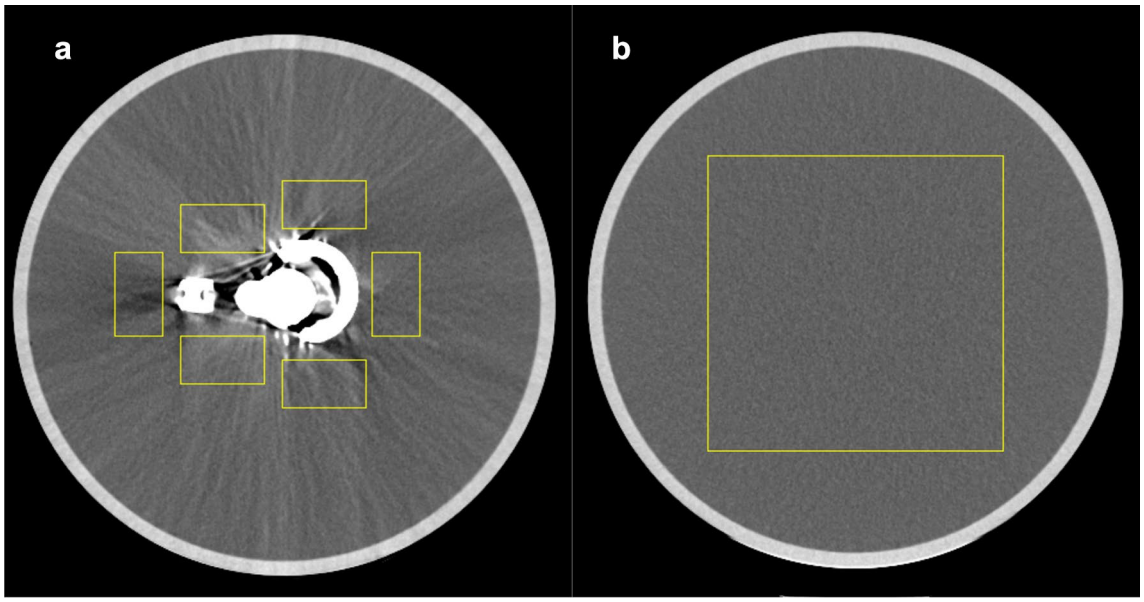

Fig. 2 The experimental setup diagram of (**a**) ROIs around the artificial hip joint and (**b**) ROI in the metal implant-free slice

Subjective image analysis

Seven radiology technologists (13 ± 5.8 years of experience, two of them were qualified as Japanese certifying organization of X-ray CT technologists for radiological technologists) were included in the subjective image analysis. All images were presented on a monochrome liquid crystal display monitor with scan data and reconstruction algorithms blinded for independent assessment of images. Total degree of artifacts was evaluated using a five-point scale (1 = no artifacts, 2 = mild artifacts, 3 = moderate artifacts, 4 = strong artifacts and 5 = extensive artifacts) [3].

Statistical analysis

Calculated values are presented as mean ± SD. Wilcoxon signed-ranks test was used to compare the C-FOVs between M and L and the reconstruction methods between FBP, AIDR3D, and AiCE. All statistical analysis was performed using the software package easy R (EZR) [14]. A P value of < 0.05 was statistically considered significant.

Results

Objective image analysis

Table 1 shows the results of objective image analysis with the AI_r. Mean AI_r of FBP, AIDR3D, and AiCE with 320 mm/500 mm C-FOVs were 10.2/10.0, 16.3/16.4, and 17.8/17.9 without SEMAR, 3.3/3.1, 2.6/2.5, and 2.3/2.0 with SEMAR, respectively. The AI_rs of all reconstruction methods with SEMAR were lower than those of AI_rs without SEMAR (P < 0.05) (Table 2). The AI_r of FBP with 500 mm C-FOV was lower than the AI_r of FBP with 320 mm C-FOV with and without SEMAR (P < 0.05) (Table 1). There were no significant differences between 320 and 500 mm C-FOVs in AI_rs of AIDR3D and AiCE. There were significant differences in all reconstruction combinations (FBP vs AIDR3D, FBP vs AiCE, and AIDR3D vs AiCE) with and without SEMAR (P < 0.05) (Table 3).

Table 1 Detailed results of objective image analysis

SEMAR	Reconstruction method	AI_r value (320 mm C-FOV)	AI_r value (500 mm C-FOV)	P value (320 vs 500 mm)
OFF	FBP	10.2 ± 3.3	10.0 ± 3.2	P < 0.05
	AIDR3D	16.3 ± 6.1	16.4 ± 6.1	n.s
	AiCE	17.8 ± 6.7	17.9 ± 6.8	n.s
ON	FBP	3.3 ± 0.4	3.1 ± 0.2	P < 0.05
	AIDR3D	2.6 ± 0.8	2.5 ± 0.6	n.s
	AiCE	2.3 ± 1.1	2.0 ± 0.5	n.s

SEMAR single-energy metal artifact reduction, *AI_r* relative artifact index, *C-FOV* calibration-field of view, *FBP* filtered back-projection, *AIDR3D* adaptive iterative dose reduction three dimensional, *AiCE* advanced intelligent clear-IQ engine, *n.s.* not significant

Subjective image analysis

Table 4 shows the results of subjective image analysis. Mean score degree of artifacts of FBP, AIDR3D, and AiCE with

Table 2 The result of significant test at SEMAR OFF and ON in AI_r value

	P value (SEMAR OFF vs ON)	
	320 mm C-FOV	500 mm C-FOV
FBP	P < 0.05	P < 0.05
AIDR3D	P < 0.05	P < 0.05
AiCE	P < 0.05	P < 0.05

SEMAR single-energy metal artifact reduction, AI_r relative artifact index, *C-FOV* calibration-field of view, *FBP* filtered back-projection, *AIDR3D* adaptive iterative dose reduction three dimensional, *AiCE* advanced intelligent clear-IQ engine, *n.s.* not significant

Table 3 The result of significant test at each reconstruction method in AI_r value

C-FOV size	Reconstruction method	With SEMAR	Without SEMAR
320 mm	FBP vs AIDR3D	P < 0.05	P < 0.05
	FBP vs AiCE	P < 0.05	P < 0.05
	AIDR3D vs AiCE	P < 0.05	P < 0.05
500 mm	FBP vs AIDR3D	P < 0.05	P < 0.05
	FBP vs AiCE	P < 0.05	P < 0.05
	AIDR3D vs AiCE	P < 0.05	P < 0.05

AI_r relative artifact index, *C-FOV* calibration-field of view, *SEMAR* single-energy metal artifact reduction, *FBP* filtered back-projection. *AIDR3D* adaptive iterative dose reduction three dimensional, *AiCE* advanced intelligent clear-IQ engine

Table 4 Detailed results of subjective image analysis

SEMAR	Reconstruction method	Artifact score (320 mm C-FOV)	Artifact score (500 mm C-FOV)	P value (320 vs 500 mm)
OFF	FBP	4.9 ± 0.4	4.9 ± 0.4	n.s
	AIDR3D	4.0 ± 0.0	4.0 ± 0.0	n.s
	AiCE	4.0 ± 0.0	4.0 ± 0.0	n.s
ON	FBP	3.9 ± 1.1	3.9 ± 1.1	n.s
	AIDR3D	3.0 ± 1.0	2.9 ± 0.4	n.s
	AiCE	2.0 ± 0.0	2.0 ± 0.0	n.s

SEMAR single-energy metal artifact reduction, *C-FOV* calibration-field of view, *FBP* filtered back-projection, *AIDR3D* adaptive iterative dose reduction three dimensional, *AiCE* advanced intelligent clear-IQ engine, *n.s.* not significant

320 mm/500 mm C-FOVs were 4.9/4.9, 4.0/4.0, and 4.0/4.0 without SEMAR, 3.9/3.9, 3.0/2.9, and 2.0/2.0 with SEMAR, respectively. There were no significant differences between 320 and 500 mm C-FOVs in all reconstructions. AiCE with SEMAR images were rated as having significantly lower score of degree of artifacts than FBP and AIDR3D with SEMAR images (P < 0.05) (Table 5).

Table 5 The result of significant test at each reconstruction method in artifact score

C-FOV size	Reconstruction method	With SEMAR	Without SEMAR
320 mm	FBP vs AIDR3D	n.s	P < 0.05
	FBP vs AiCE	P < 0.05	P < 0.05
	AIDR3D vs AiCE	P < 0.05	n.s
500 mm	FBP vs AIDR3D	n.s	P < 0.05
	FBP vs AiCE	P < 0.05	P < 0.05
	AIDR3D vs AiCE	P < 0.05	n.s

C-FOV calibration-field of view, *SEMAR* single-energy metal artifact reduction, *FBP* filtered back-projection. *AIDR3D* adaptive iterative dose reduction three dimensional, *AiCE* advanced intelligent clear-IQ engine, *n.s.* not significant

Discussion

This study evaluated the effects of SEMAR for metal artifacts using CT images reconstructed with DLR and IR in different C-FOV sizes. In the objective evaluation, there were no significant differences between 320 and 500 mm C-FOVs in AI_rs of AIDR3D and AiCE. In the subjective evaluation, there were no significant differences between 320 and 500 mm C-FOVs in all reconstructions. We found that the effect of SEMAR for metal artifacts using CT images reconstructed with AIDR3D and AiCE are not altered by the C-FOV sizes.

In this study, using SEMAR reduced AI_r value and improved the subjective score of metal artifact with all reconstruction methods and all C-FOV sizes. Various authors have indicated that the SEMAR can reduce metal artifacts in patients with orthopedic prostheses [1, 5–7], endovascular aortic repair devices [11], pacemaker [3], dental prostheses [6, 8], and embolization coils [6] under a variety of image acquisitions. Similarly, we considered that SEMAR could improve image quality with reduced metal artifacts in CT images with all reconstruction methods and all C-FOV sizes.

Focusing on the change of C-FOV sizes, the AI_r of FBP was affected by C-FOV sizes. It has been reported that the metal artifact-reducing effects of SEMAR using FBP is affected by C-FOV sizes, supporting the result of this study [7]. we considered this to be due to the bow-tie filter and the number of detectors in a CT instrument used in this study depend on the C-FOV sizes. The X-ray effective energy of 320 mm C-FOV is higher than that of 500 mm C-FOV because of differences in the bow-tie filter [15]. We considered that the high X-ray effective energy caused beam hardening that read to reducing the number of photons reaching the detector and increasing the metal artifacts of 320 mm C-FOV. Furthermore, we considered that the change in the synogram with the change in the

number of detectors affected the reconstruction process of SEMAR.

In the other hand, the AI_r of AIDR3D and AiCE were not affected by C-FOV sizes. This result in the AI_r of AIDR3D could be attributed to the effect of AIDR3D for noise or artifact reduction and the creation of new artifacts [5]. The creation of new artifacts when using SEMAR combined with AIDR3D has previously been reported [5]. In the AiCE, we considered that this result in the AI_r of AiCE was obtained because the teacher data used in the AiCE reconstruction process may be the same regardless of the C-FOV sizes. However, it remains unclear how the SEMAR reconstructed images will be affected when SEMAR is combined with AIDR3D or AiCE.

In this subjective study, there were no significant differences in the metal artifact scores between 320 and 500 mm C-FOVs with all reconstructions. We considered that the metal artifact reduction effect of CT images reconstructed with AiCE and AIDR3D, which showed no significant differences in C-FOV sizes in both objective and subjective image analysis, may not be affected by C-FOV sizes. The AI_r value and the metal artifact score using SEMAR combined with AiCE were lower than combined with other reconstruction methods. Therefore, the optimal choice of reconstruction methods for metal artifact reduction may be with SEMAR combined with AiCE.

This study has limitations. First, this phantom was composed without bones or hip joint on the other side and did not account for the effect of body shape. More accurate assessment, taking into account the effect of body shape and streak artifacts with hip joints on the both sides, may be obtained using an anthropomorphic phantom with a simulated bones and hip joint on both sides. Second, we used a single CT scanner in this study. The image reconstruction process may be different for each CT vendors. The effect of metal artifact reduction is dependent on the reconstruction algorithm of each CT vendors [5]; therefore, it does not always show the same results as this study.

Conclusion

In conclusion, SEMAR enabled a significant reduction of metal artifact caused by the artificial hip joint in all reconstruction methods and C-FOV sizes. SEMAR combined with AiCE more effective at reducing metal artifacts than SEMAR combined with FBP or AIDR3D. In the SEMAR combined with FBP, the effect of metal artifact reduction was affected by C-FOV sizes. In the SEMAR combined with AIDR3D or AiCE, the effect of metal artifact reduction was not affected by C-FOV sizes.

Acknowledgements The authors thank all the radiological technologist at Gero Hot Spring Hospital for their advice and assistance throughout this study.

Author contributions KT contributed to the study design, data collection, and writing and editing of this article; NO contributed to the study design, data collection, and reviewing of this article; YO, KT, and MK contributed to the project administration and reviewing of this article. All authors read and approved the final manuscript.

Funding The authors declare that no funds, grants, or other support were received during the preparation of this manuscript.

Code availability Not applicable.

Declarations

Competing interest The authors have no relevant financial or non-financial interests to disclose.

Ethical approval This study was performed in line with the principles of the Declaration of Helsinki. Approval was granted by the Hospital Ethics Committee (May 6, 2021; No.48).

Informed consent Informed consent was obtained from all individual participants (visual evaluators) included in this study.

References

1. Gondim Teixeira PA, Meyer JB, Baumann C, Raymond A, Sirveaux F, Coudane H et al (2014) Total hip prosthesis CT with single-energy projection-based metallic artifact reduction: impact on the visualization of specific periprosthetic soft tissue structures. Skeletal Radiol 43(9):1237–1246
2. Barrett JF, Keat N (2004) Artifacts in CT: recognition and avoidance. Radiographics 24(6):1679–1691
3. Kikuchi N, Yanagawa M, Enchi Y, Nakayama A, Yoshida Y, Miyata T et al (2020) The effect of the reconstruction algorithm for the pulmonary nodule detection under the metal artifact caused by a pacemaker. Medicine 99(24):e20579
4. Wang Y, Qian B, Li B, Qin G, Zhou Z, Qiu Y et al (2013) Metal artifacts reduction using monochromatic images from spectral CT: evaluation of pedicle screws in patients with scoliosis. Eur J Radiol 82(8):e360–e366
5. Andersson KM, Nowik P, Persliden J, Thunberg P, Norrman E (2015) Metal artefact reduction in CT imaging of hip prostheses-an evaluation of commercial techniques provided by four vendors. Br J Radiol 88(1052):20140473
6. Sonoda A, Nitta N, Ushio N, Nagatani Y, Okumura N, Otani H et al (2015) Evaluation of the quality of CT images acquired with the single energy metal artifact reduction (SEMAR) algorithm in patients with hip and dental prostheses and aneurysm embolization coils. Jpn J Radiol 33(11):710–716
7. Tsuboi K, Fukunaga M, Yamamoto H (2016) The effect of metal artifact reduction at different calibrated and display field of views in computed tomography. Nihon Hoshasen Gijutsu Gakkai zasshi. 72(12):1237–1244 (**In Japanese**)
8. Yasaka K, Kamiya K, Irie R, Maeda E, Sato J, Ohtomo K (2016) Metal artefact reduction for patients with metallic dental fillings in helical neck computed tomography: comparison of adaptive iterative dose reduction 3D (AIDR 3D), forward-projected model-based iterative reconstruction solution (FIRST) and AIDR

3D with single-energy metal artefact reduction (SEMAR). Dentomaxillofac Radiol 45(7):20160114
9. Wei F, Li J, Zhou C, Li Y, Wang X, Huang B et al (2020) Combined application of single-energy metal artifact reduction and reconstruction techniques in patients with Cochlear implants. J Otolaryngol Head Neck Surg 49(1):1–9
10. Kawahara D, Ozawa S, Yokomachi K, Higaki T, Shiinoki T, Saito A et al (2019) Metal artifact reduction techniques for single energy CT and dual-energy CT with various metal materials. BJR Open. 1(1):bjro-20180045
11. Ragusi MAAD, van der Meer RW, Joemai RMS, van Schaik J, van Rijswijk CSP (2018) Evaluation of CT angiography image quality acquired with single-energy metal artifact reduction (SEMAR) algorithm in patients after complex endovascular aortic repair. Cardiovasc Intervent Radiol 41(2):323–329
12. Abramoff MD, Magalhaes PJ, Ram SJ (2004) Image processing with ImageJ. Biophotonics Int 11(7):36–42
13. Takada K, Ichikawa K, Banno S, Otobe K (2018) Suggestion of the relative artifact index for noise-independent evaluation of the streak artifact. Nihon Hoshasen Gijutsu Gakkai zasshi. 74(4):315–325 (**In Japanese**)
14. Kanda Y (2013) Investigation of the freely available easy-to-use software 'EZR' for medical statistics. Bone Marrow Transplant 48(3):452–458
15. Kuramochi K, Ogawa Y, Chikaraishi K, Tateishi K, Yoshikawa T (2013) Usefulness of low kilovoltage settings in computed tomography venography of lower limbs. Nihon Hoshasen Gijutsu Gakkai zasshi. 69(1):85–91 (**In Japanese**)